Structural Models and Thermal Desorption Energetics for Multilayer Assemblies of the *n*-Alkanes on Pt(111)

Adeana R. Bishop, Gregory S. Girolami, and Ralph G. Nuzzo*

Departments of Chemistry and Materials Science and Engineering and the Frederick Seitz Materials Research Laboratory, University of Illinois at Urbana-Champaign, Urbana, Illinois 61801

Received: July 28, 1999; In Final Form: October 30, 1999

The structural and thermodynamic properties of linear hydrocarbon multilayer assemblies supported on a Pt(111) single-crystalline substrate are investigated with temperature-programmed desorption and infrared reflection absorption spectroscopies. The multilayer assemblies are comprised of all-trans chains preferentially aligned with their *ccc* planes parallel to that of the surface. Coverage-dependent vibrational spectra reveal that the deposition process, up to the first monolayer total coverage, proceeds first via an island growth mechanism. This result demonstrates that an important contribution is made by (chain-length-dependent) attractive lateral interactions to the binding energies of the monolayer films. The subsequent layers deposited in a multilayer appear to contain a modest concentration of conformational/orientational defects (and perhaps layer misplacements as well). The energetics of the desorption processes for these hydrocarbon assemblies are rationalized on the basis of a conserved value of a prototypical segmental heat of adsorption. The kinetic model embodying this description involves a layer-by-layer desorption and invokes a central role for lateral interactions and diffusion in maintaining the kinetic competence of a general mechanism of monolayer evaporation from two-dimensional island domains.

Introduction

There exists a growing interest in the properties exhibited by low-dimensional organic thin films and materials. For example, considerable efforts have been made to develop a deeper understanding of the structures and thermally driven phase transitions seen in such important systems as lipid bilayers,[1] surfactant interfaces,[2] Langmuir−Blodgett films,[3,4] and self-assembled monolayers,[5,6] as but a few examples. Despite this effort, the conformational dynamics of even simple organic thin-film assemblies remain poorly understood. In part for these reasons, the structures adopted by alphatic hydrocarbons, and the dynamics underlying their phase transitions, have become a model system of much interest, and great efforts have been made to determine their character in both bulk solid[7−11] and liquid states,[12] as well as in thin-surface-boundary-layer phases.[13,14]

A vast literature has been collected that describes the nature of the complex structural phase transitions exhibited by hydrocarbons in bulk.[15−26] A number of interesting insights can be gleaned from this material. For example, odd-chain-length *n*-alkanes of between 9 and 45 carbon segments are known to undergo at least one premelting phase transition,[27] and longer hydrocarbons have been reported to exhibit as many as five distinct plastic-crystalline phases between the ordered crystalline and isotropic liquid phases.[17] All of these phases are characterized by weak interlayer coupling and the transitions between them by large changes in structural constants as a function of temperature (diverging critically at the phase boundary).[23] It is interesting to note that one of the structural transitions seen in the bulk systems, the so-called rotator phase transition,[15−26] appears to have a close correspondence to the premelting[28−30] behaviors observed in thin films. It also is observed that (where possible) mixing hydrocarbon chains of different lengths results in a lowering of rotator phase transition temperature; the range over which this transition occurs is found to increase with the magnitude of the differences in the chain length.[18] The mixed bulk hydrocarbons exhibit increased conformational (predominately chain-end) defects (e.g., gauche and kink conformations) and longitudinal displacements (to reduce void volume and surface roughness, which results in a packing structure similar to the high-temperature hexagonal structures seen in pure *n*-alkanes).[31]

In this report we present the results of a detailed study on the chain-length-dependent phase properties of ordered thin-film assemblies of the *n*-alkanes supported on a single-crystalline Pt(111) substrate. An overview of the structural and thermodynamic properties of hydrocarbon monolayers and bilayers on Pt(111) is given. A central focus of this study is a critical evaluation of the rate/structure correlations evidenced in temperature-programmed desorption (TPD) studies, which shed light on the nature of their surface binding interactions and phase dynamics, factors which in turn complicate the interpretation of such data. Of particular concern in this report is the suggestion that stabilizing lateral interactions play a major role in determining the nature of the kinetics of desorption from the monolayer bound state. A simple (limiting) kinetic model that invokes facile lateral diffusion and attractive interactions with neighbors, and thus accounts qualitatively for the contributions made by the phase dynamics to the mechanism of desorption, is presented. Using the results of TPD and reflection absorption infrared (RAIR) spectroscopies, we present simulations based on the simplest version of the model that rationalizes the rate/structure sensitivities of the desorption processes of surface-bound hydrocarbon assemblies in terms of a physically plausible average surface−segment interaction energy (one that is conserved for a series of *n*-alkane adsorbates of varying chain lengths). The microscopic bases for the model are found to

* To whom correspondence should be addressed.

10.1021/jp9926488 CCC: $19.00
Published on Web 01/05/2000

follow naturally from insights gained in an earlier study focusing on the dynamics of self-diffusion in these systems.[32]

Experimental Method

All experiments were performed in ultrahigh vacuum using methods that have been described previously,[33] and only a brief overview is given here. Reflection adsorption infrared spectroscopy (RAIRS) studies were performed in a stainless steel vacuum chamber equipped with turbomolecular, ion, and titanium sublimation pumps, temperature-programmed desorption (TPD), and Auger electron spectroscopies (AES) and having a base pressure of $<3.0 \times 10^{-10}$ Torr. The Pt(111) crystal was cleaned before each experiment by heating it in a 1.0×10^{-6} Torr atmosphere of dioxygen at 980 K for 5−8 min and subsequently annealing it at 1070 K. The exposures were made form the background and were calibrated (for the ion gauge sensitivity) by RAIRS as described elsewhere.[32] To form a well-ordered monolayer, the Pt(111) crystal was cooled to a temperature lying between the monolayer and the multilayer desorption temperatures for the specific hydrocarbon being studied and exposed to the equivalent of several tens of monolayers at this temperature. The temperatures used for the various chain-length hydrocarbons studied are hexane, 170 K; heptane, 185 K; octane, 190 K; nonane, 205 K; decane, 230 K. After dosing, the pressure was allowed to recover before the crystal was cooled to 110 K, at which point subsequent components could be dosed and a controlled coverage in the multilayer formed. At this temperature, the partial pressure of the surface-bound component is negligible and the second component adsorbs only on the hydrocarbon precovered surface.

The linear alkanes hexane (99+%), heptane (99%), octane (99+%), octane-(d_{18}) (98+%), nonane (99%), and decane (99+%) were purchased from Aldrich and purified by the freeze−pump−thaw cycling method.

RAIR spectra were taken with a Bio-Rad FTS-60A spectrophotometer aligned with *f*/15 optics at a near grazing incidence angle, 85° from the surface normal. A total of 1024 or 4096 scans were coadded with a resolution of 4 cm^{-1}.[34]

TPD spectra were obtained with a VG Quadrupole SXP 300 mass analyzer differentially pumped by a 60 L/s ion pump. The sample temperature and ramp rate were controlled by a Eurotherm temperature controller and a Lambda programmable power supply. Linear temperature program ramp rates of 2 K/s were used unless otherwise specified. Data were acquired with a 12 bit analog-to-digital converter on a 486 personal computer running LabTech software.

Results and Discussion

Infrared Spectroscopy. The dipole selection rule, which determines the modes observable by RAIRS for adsorbates bound on metallic surfaces, was utilized to deduce the average molecular orientations adopted by the hydrocarbon chains on the Pt(111) substrate.[35,36] Owing to the reflection of the electromagnetic field at the metal surface, dynamic dipole moments with components aligned parallel to the surface normal direction will have enhanced intensities while those with only perpendicular contributions will show no intensity in the resulting RAIR spectra.[35,36] Of further concern, C−H interactions with the metal surface result in significant mode softening, and the intensities of these features exhibit sizable red-shifts relative to the frequencies seen in their isotropic spectra, an effect which facilitates the differentiation of surface-bound and nonsurface-bound segments. Taken together, these effects provide a sensitive basis for determining molecular orientations

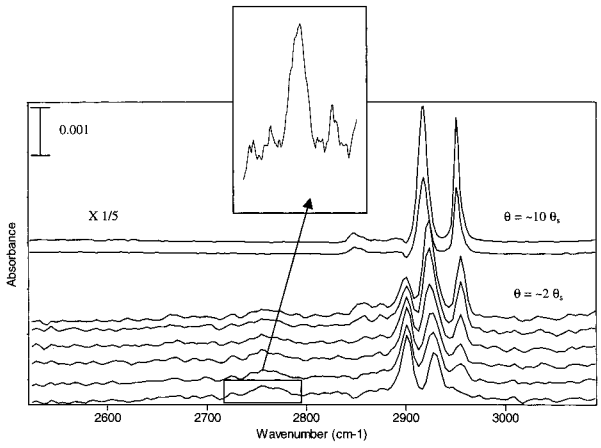

Figure 1. RAIR spectra of octane on Pt(111) showing changes in the vibrational spectra in the C−H stretching region with increasing multilayer coverage.

present in a bilayer assembly (a limiting coverage of primary interest here) but also can provide valuable information regarding the relative positions of the molecules in a multicomponent assembly.[33]

Representative RAIR spectra of octane adsorbed on Pt(111) are shown in Figure 1. These spectra were acquired in two parts: first, after successive exposures of the Pt(111) surface to octane vapor at 180 K until a limiting coverage of ∼1 monolayer ($\theta = 1.0\theta_s$) was reached; second, after further exposures to octane vapor at 110 K until a limiting coverage of ca. 10 monolayers ($\theta = 10\theta_s$) was reached. The spectra of the monolayer are consistent with an organization of a single molecular layer comprised of all-trans chains lying with the plane of the carbon atoms parallel to that of the surface, a result firmly established by earlier LEED[13] and RAIRS studies.[29,32,37] The multilayer spectra suggest that a similar, but somewhat more defective, arrangement of chains is present in the second layer (see below). The inset to the figure shows an expanded view of the mode softening seen for the monolayer at 110 K for a separate acquisition optimized for their visualization. The mode assignments for these spectra, which have been summarized elsewhere,[29,32,37] are reviewed in Table 1. We should point out explicitly at this point that all of the C−H stretching modes of the surface-contacting chains are highly perturbed and show large frequency shifts in the "normal" C−H stretching region. They are further complicated by the appearance of multiple bands for C−H stretching motions of the methyl and methylene groups, which cannot be rationalized in the context of any molecular arrangement of an unperturbed chain, and substantial mode softening as evidenced by the appearance of a broad set of bands in the 2700−2800 cm^{-1} region.[37] The carbon−hydrogen stretching modes at 2900 (methylene), 2929, and 2947 cm^{-1} are the most intense features that arise from the methylene and methyl groups interacting with the surface (Table 1). These modes, being affected by the interaction with the surface, are red-shifted relative to unperturbed C−H modes. The broad features predominately centered at 2756 cm^{-1} are softened modes due to direct C−H···M interactions.[37] The lower six RAIR spectra presented in Figure 1 correspond to the monolayer (bottom) and multilayers formed by the sequential addition of a fractional coverage of the adsorbate equivalent to one-third of a layer. The top two spectra result from the addition of a total of approximately 5 and 10 layers and are scaled by a factor of $^1/_5$. The mode assignments in the C−H stretching region for the chains in the multilayer follow simply from those expected on the basis of the normal modes of an unperturbed *n*-alkane.[38]

TABLE 1: Mode Assignments for *n*-Octane on Pt(111)

	CH_3 δ(C−H)	CH_2 δ(C−H)	ν(C−$H_{proximal}$)[a]	CH_2 ν(C−H_{distal})[b]	CH_3 ν(C−H_{distal})[b]	CH_2 d^-	ν(C−H)[38] d^+	CH_3 r^-	ν(C−H)[38] r^+
n-octane monolayer			2669, 2758, 2818	2896, 2903	2928, 2947				
n-octane multilayer	1380	1457, 1469				2917	2851	2953	2873

[a] The C−H bond contacting the surface. [b] The C−H bond projecting away from the surface.

The multilayer spectra are dominated by two intense bands (neglecting those due to surface-contacting chains): the antisymmetric methyl stretch, r^-, at 2951 cm^{-1} and the antisymmetric methylene stretch, d^-, at 2917 cm^{-1} (as expected for an assembly of all-trans chains aligned with their *ccc* plane parallel to that of the surface). Modest intensity is also noted for modes corresponding to the methylene symmetric, d^+, and methyl symmetric, r^+, C−H stretching modes (2853 and 2873 cm^{-1}, respectively). The intensities of these latter modes, being weak and scaling nonlinearly with coverage, suggest that they originate in chains exhibiting orientational defects. These defects must exhibit a rotation of the *ccc* plane out of coplanarity with the surface. The d^+ mode shows a poorly resolved splitting of ~9 cm^{-1}. The methylene bending mode (not shown) demonstrates a similar behavior (with component features of nearly equal intensity appearing at 1459 and 1469 cm^{-1}). We believe these splittings may arise from factor group interactions. Related splittings of methylene bending and rocking modes are well-documented in the literature on crystalline orthorhombic phases of polyethylene[39,40] and long-chain hydrocarbons[41−43] but, to our knowledge, have not been observed for the d^+ modes of bulk solids (such splittings have been seen in alkanethiol SAMs on Au, however).[6] This splitting is indicative of an intermolecular coupling and, with a few assumptions, can be used to analyze the packing structure of the orientational defects of the molecules.[41,44] In analogy with a bulk phase, the nearly equal intensity of the two components suggests a setting angle in a two-chain orthorhomic subcell of ~90 (i.e., an orthogonal arrangement of the *ccc* planes in a two-chain unit cell). This bulk inspired model of the local defect structure does present several problems, however. The greatest concern arises from the assumed nature of the growth processes. If the growth of the multilayer were to proceed on a layer-by-layer basis, the symmetry of a bulklike orthorhombic sublattice could not be obtained at bilayer coverages and thus the splittings would have to follow from interactions occurring in some other multichain habit. It should be noted that the binding enthalpy of the second layer will differ only slightly from that of the higher surface layers, and as such substantial deviations from a sequential layer growth process are to be expected after the first monolayer. A test is needed to determine rigorously if the observed features are due to factor group splitting or some other cause. Isotopic dilution experiments were performed toward this end. In these experiments, either octane-h_{18} or an equal mixture of octane-d_{18} and -h_{18} was dosed at 97 K[45] onto a Pt(111) surface precovered with a saturation monolayer of the d_{18} isotopomer. The apparent splittings, as illustrated by the pattern of d^+ modes shown in Figure 2, remained all the same. While considerable uncertainty remains, we believe the best explanation is that the growth occurring beyond the monolayer is not rigorously layer-by-layer but proceeds via the formation of three-dimensional clusters supported on a dense monolayer (a Stranski−Krastinov growth habit). At the low temperatures used in this experiment, isotopically driven phase segregation of the *n*-C_8 chains is expected within the island domains. Auger electron spectroscopy studies were also conducted to examine the growth mechanism,[46,47] but the layers were severely degraded by the electron beam and thus could not be analyzed in this way.

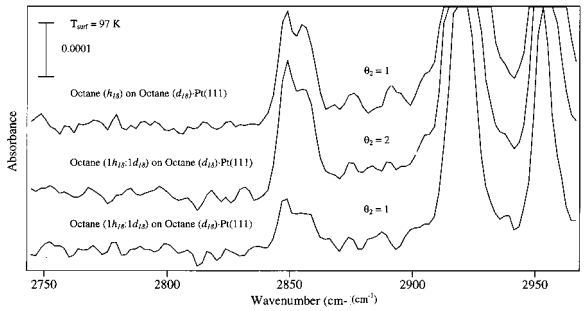

Figure 2. Change in the line shape of the defect methylene symmetric stretching mode seen in a multilayer with changes in isotopic dilution and coverage in the multilayer.

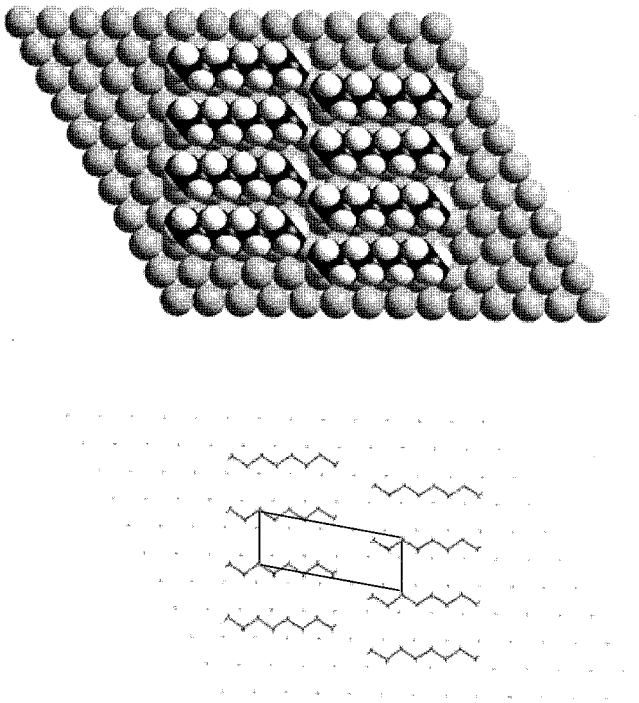

Figure 3. Schematic structure of a monolayer of *n*-octane on Pt(111).

Firment and Somorjai[13] have shown by LEED that the surface mesh of an *n*-octane multilayer structure on Pt(111) does not change from that observed for the monolayer structure, and further propose that it is similar to the (101) plane of the monoclinic bulk structure.[7] Figure 3 shows this proposed structure for the *n*-octane monolayer on Pt(111). As shown in the figure, the dimensions of this single-chain unit cell are 4.80 Å by 12.7 Å, with an included angle of 79°. There are several plausible structures for a multilayer that can rationalize all the data obtained by RAIRS[29,32,37] and LEED.[13] Molecular Simulations derived graphics are shown in Figures 4−6, which illustrate the essential features of the likely structural motif, restricting our consideration to an overly simplified case of the tiling seen in a bilayer. The simulations suggest that the rough corrugation of the monolayer is best matched when the chains tiling the second layer are staggered relative to the first. The data are

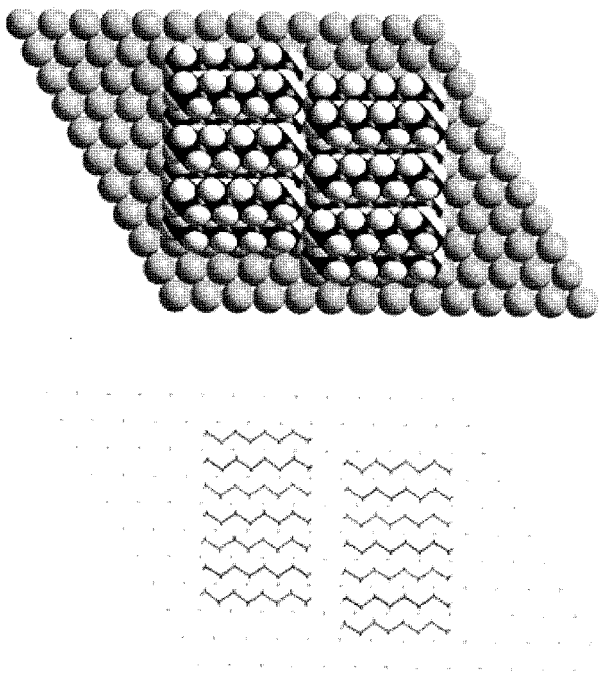

Figure 4. Schematic depiction of a possible bilayer structure of octane on Pt(111). Details are described in the text. In the figure, surface-contacting chains are shown with lighter shading.

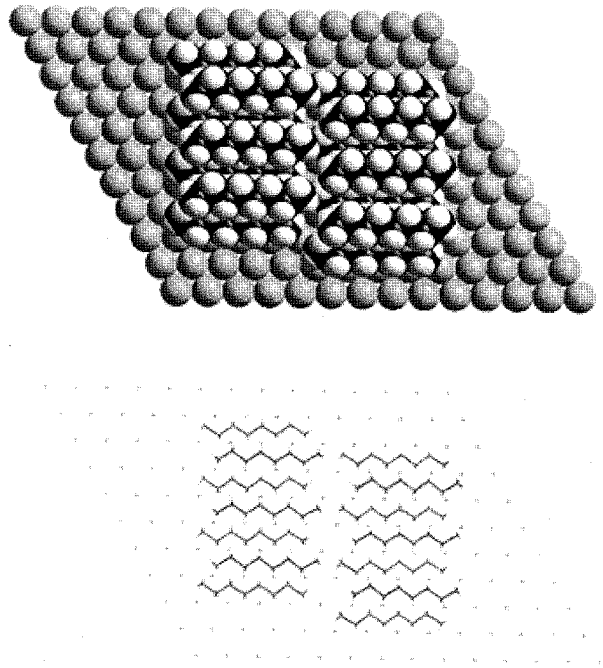

Figure 5. Schematic depiction of a possible bilayer structure of octane on Pt(111). Details are described in the text. In the figure, surface-contacting chains are shown with lighter shading.

less clear as to the organization of the internal methyl surface, but it seems likely that motifs reminiscent of either monoclinic (Figure 4) or triclinic (Figure 5) phases could be obtained (the latter via a slip of the second layer chain along the trough of the underlying monolayer). The special case shown in Figure 6 depicts the structure created when the multilayer molecules retain the same symmetry relative to the platinum substrate as that found in the monolayer.

Temperature-Programmed Desorption. The desorption kinetics for layers formed by a homologous series of hydrocarbons (hexane through decane) were examined by tempera-

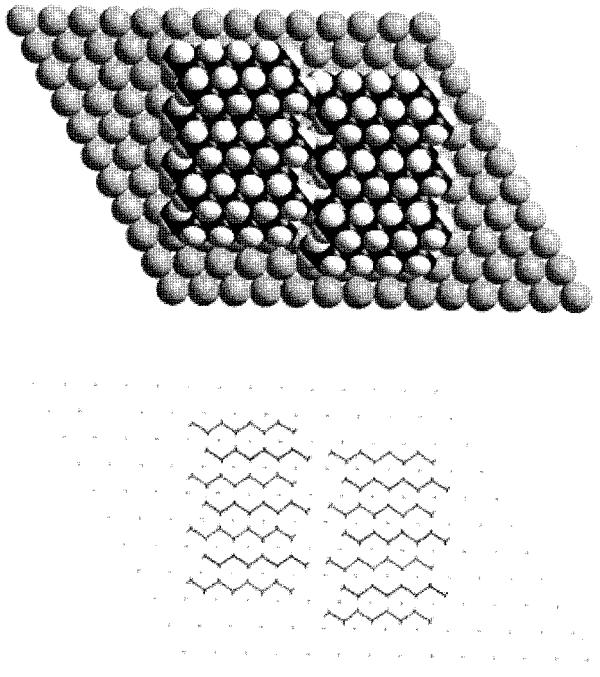

Figure 6. Schematic depiction of a possible bilayer structure of octane on Pt(111). Details are described in the text. In the figure, surface-contacting chains are shown with lighter shading.

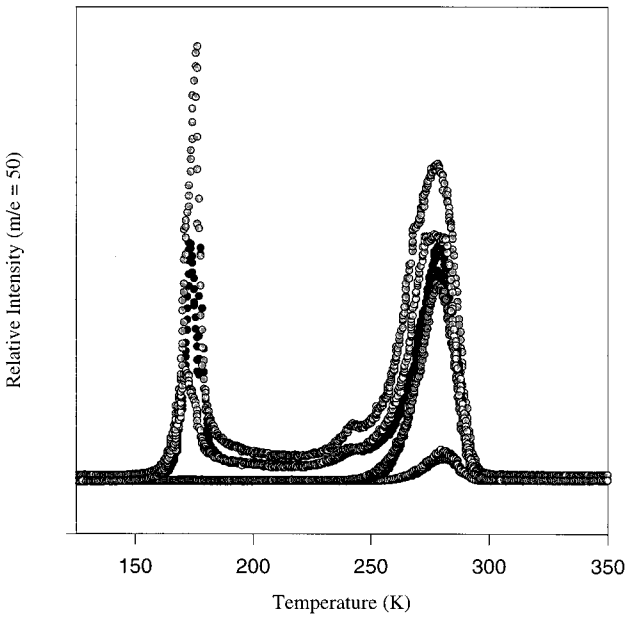

Figure 7. TPD spectra of octane-d_{18} on Pt(111) showing changes in line shape with increasing coverages.

ture-programmed desorption. These spectra show two general desorption features for coverages exceeding a monolayer; the temperatures at which these peaks appear scale with the chain length of the adsorbate. Figure 7 shows representative spectra obtained for octane-d_{18} on Pt(111) at varying coverages. The lower temperature desorption feature corresponds to molecules present in a multilayer, while the higher temperature feature corresponds to the desorption of chains more tightly bound in the monolayer.

Figure 8 shows desorption spectra for a series of multilayers comprised of hexane, heptane, and octane at formal coverages on Pt(111) below that of a bilayer. The data show that as the chain length increases, so does the peak-maximum desorption temperatures for both the multilayer and surface-bound species.

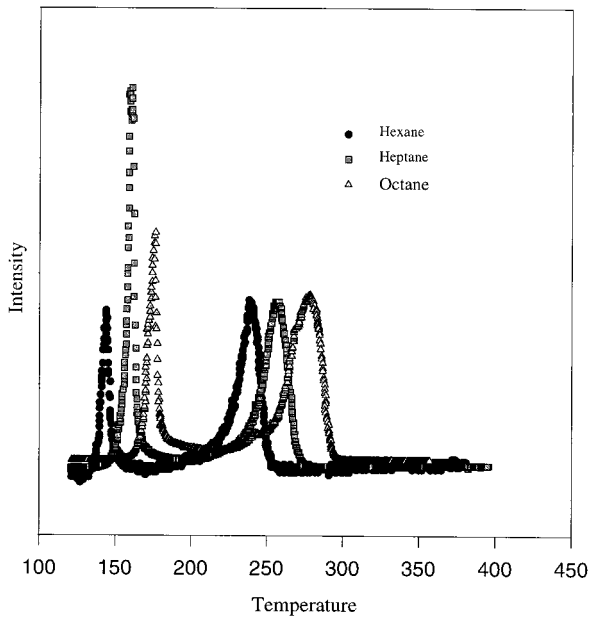

Figure 8. TPD spectra showing desorption of hexane, heptane, and octane from Pt(111). The low-temperature feature corresponds to desorption from the multilayer; the high-temperature feature is desorption from the monolayer. For the series C_6-C_8, the ions followed were $m/e = 43$.

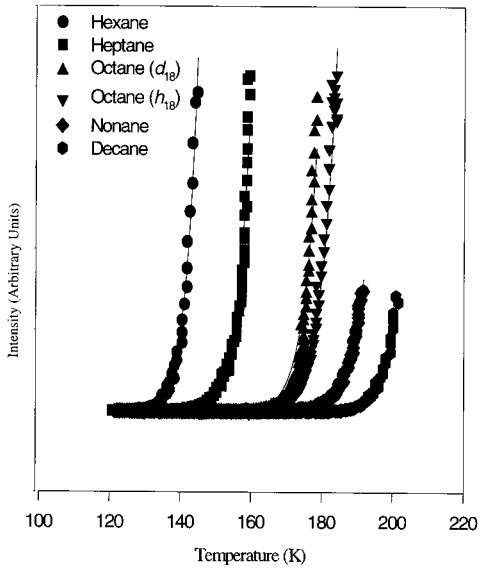

Figure 9. Zero-order desorption fits to the leading edge of the multilayer desorption features for the series of hydrocarbons hexane through decane.

Also notable is the difference in line shape between the two desorption features seen in each spectrum. These line shape differences are consistent with underlying differences in the descriptive rate laws such as might exist for zero-order and first-order desorption processes.[48−50] These assumptions do present some problems when invoked to explain the quantitative aspects of the rate/structure correlations seen in the chain-length dependencies. We turn to a consideration of these aspects immediately below.

Kinetic Modeling. Desorption form a multilayer state is most simply described by a zero-order rate law. The suitability of this analytical construct to the systems of interest here is supported by the observed invariance of the leading edge of the TPD trace for this state to changes in the coverage of the adsorbate.[46,48−50] The quantitative analysis of the TPD data for the nonsurface-contacting species thus can be accomplished by fitting the leading edge of the desorption traces with a simple exponential rise. The activation energy for desorption (a term potentially related to the heat of sublimation, see below) can be calculated by fitting the intensity profile to the equation

$$I = \nu \exp(-\epsilon/RT)$$

where the constants ν and ϵ are the preexponential factor (and other collected constants that enter nonexponentially) and the activation energy, respectively. Figure 9 shows a series of fits made in this way to data extracted from the multilayer leading edge profiles for several hydrocarbons. The fitting parameters obtained are given in Table 2. The values of the chain-length-dependent activation energies (ϵ) scale in a qualitatively sensible way (see below). The values of ν, however, are nonphysical if related directly to a preexponential factor.[51] The measured values for the chain-length-dependent multilayer desorption activation energies are compared in Figure 10 with energies calculated from literature values for the heats of fusion and vaporization in the bulk at 25 °C.[52] We see a reasonable correspondence between the energies calculated in this way and the values of the bulk thermodynamic properties (i.e., the chain−chain interaction energies). This agreement supports the validity of the kinetic approximation used to model the TPD data.

An alternate presentation of the data shown in Figure 10 proved to be instructive. By taking the desorption activation energies calculated from the fits to a zero-order rate law for the desorption and dividing them by the chain length, we obtain

TABLE 2: Fitting Parameters Calculated from a Zero-Order Rate Law Corresponding to Desorption Activation Energies for Multilayer Desorption Data[a]

hydrocarbon	fitting parameter ν_1[54]	desorption energy (kcal/mol)	heat of sublimation calcd from lit[52]
hexane	1×10^{20}	12.8	10.6687
heptane	1×10^{20}	14.1	12.1252
octane	1×10^{20}	16.2	14.8523
nonane	1×10^{20}	17.3	14.7899
decane	1×10^{20}	18.2	19.1577

[a] The literature values for comparison are obtained from the heats of fusion and heat of vaporization for bulk alkanes.

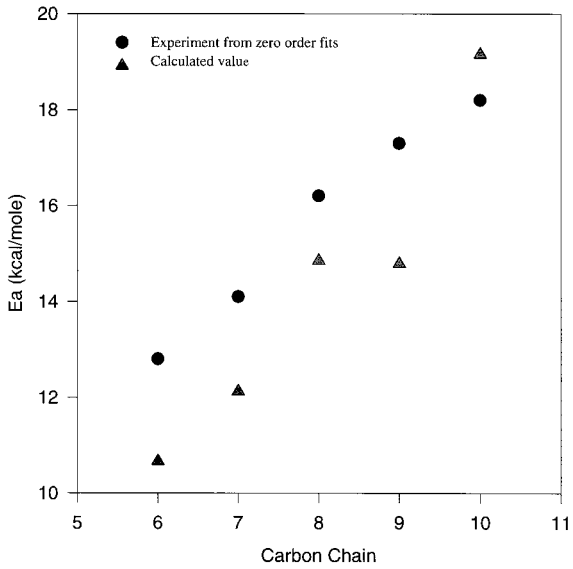

Figure 10. Enthalpies of sublimation for a series of *n*-alkanes at 25 °C calculated from literature values (▲) and the desorption activation energies for these same species in a multilayer as calculated from a zero-order rate analysis.

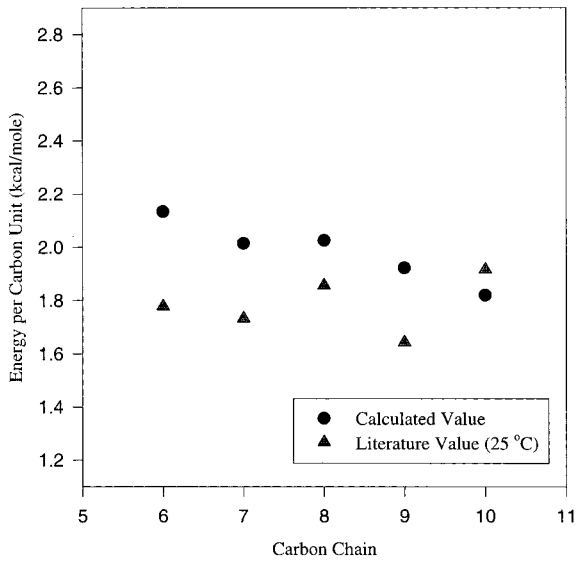

Figure 11. Activation and sublimation energies per carbon segment calculated for the data shown in Figure 10.

the plot shown in Figure 11. As can be seen by inspection of these data, the chain−chain segmental interaction energy for the multilayer (as deduced from TPD) is fairly constant, yielding a value centered at about 2 kcal/mol for the chain lengths studied. The systematic decrease seen with increasing chain length is modest and we believe reflects (in part, see below) limitations in the measurement protocol. The average value of the chain−chain segmental interaction energy, again, closely follows data for bulk hydrocarbons.

Related investigations of the desorption of multilayers of various *n*-alkanes on Cu(100) gave the following values for the desorption activation energies: pentane, 10.4 kcal/mol; hexane, 12.0 kcal/mol; heptane, 13.6 kcal/mol; octane, 14.6 kcal/mol; nonane, 16.2 kcal/mol; decane, 17.9 kcal/mol.[53] When normalized for chain length, these values give significantly varying estimates of the chain−chain segmental interaction energies of 2.09, 2.00, 1.95, 1.82, 1.80, and 1.79 kcal/mol for the series, respectively.

The analysis of the desorption kinetics for the monolayer states presents a more complex set of issues. As a starting point, an evaluation made in the context of a first-order rate law seems most sensible. Using the individual monolayer peak desorption temperatures (T_p), the activation energy of the desorption process for each chain length can be calculated from the equation given by Redhead[54]

$$\frac{E}{RT_p} = \ln \frac{\nu_1 T_p}{\beta} - 3.64 \qquad (2)$$

where T_p is the temperature at which the desorption rate is at a maximum, ν_1 is the preexponential factor (for which a value $\approx 1 \times 10^{13}\ s^{-1}$ is typical), and β is the heating rate. By assuming a "normal" value for the preexponential factor and for the heating rate of 2 K/s used in these experiments, values of the desorption energies can be calculated for each chain length; the results obtained for saturation exposures are given in Table 3 for each hydrocarbon. Figure 12 shows a plot of the chain-length dependence of the desorption activation energy calculated in this way. Again, it is useful to consider the magnitude of the segmental interaction energy suggested by these data. To do so, it is instructive to normalize the desorption energy for each hydrocarbon by the number of carbon atoms; these data are plotted against the right axis of Figure 12. This analysis at its most simplistic level (see below) suggests that the average activation energy needed to remove a chain segment from the Pt surface decreases markedly with increasing chain length. Such trends are not seen in theoretical predictions of the average segmental interaction energies calculated for hydrocarbons on Pt or group constituent heats of sublimation found for the bulk phases of hydrocarbons (which remain nearly constant at approximately 1.8 kcal/mol per segment).[52]

TABLE 3: Activation Energies for Monolayer Desorption Data Calculated from a First-Order Rate Law[a]

molecule	T_p (K)	E_a (kcal/mol)[52]	E_a (kcal/mol) per carbon
hexane	239.43	14.7870	2.4644
heptane	256.36	15.8676	2.2668
octane	277.43	17.2151	2.1519
nonane	285.63	17.7407	1.9712
decane	296.86	18.4606	1.8461

[a] As can be seen by the increasing surface−segmental activation energies, this analysis inadequately accounts for the desorption process.

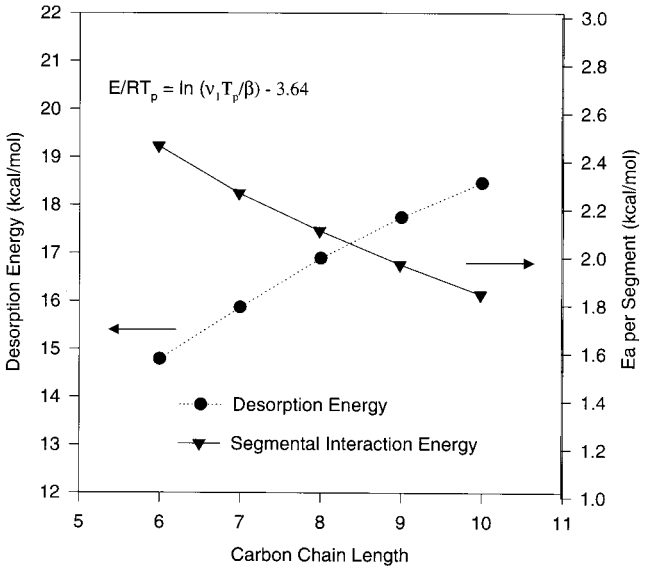

Figure 12. Scaling of the desorption energy calculated from first-order fits (left axis) and average surface-chain segmental interaction energy (right axis) as a function of chain length.

We strongly believe that the latter result (as illustrated in Figure 12) is nonphysical for several reasons. First, the values of the desorption activation energies calculated in this way are far too low. For example, the first-order fit gives a desorption energy of 17.2 kcal/mol for octane, which seems very unreasonable given that the calculated desorption energy of octane molecules from the multilayer is ~16.2 kcal/mol. For the hydrocarbon adsorbates investigated here, there must exist a sizable energy difference between these two desorption processes. A second insight (one directly related to these energies) comes from comparing the group constituent desorption energies for the two states across the entire series. This analysis suggests that the average segmental interaction energy is strongly chain-length-dependent and, for long chains on Pt(111), actually becomes smaller than the group constituent heat of sublimation. This anomaly cannot be rationalized by assigning differing values to methyl and methylene surface interactions (see below).

Desorption energies calculated by the first-order desorption model for related systems have yielded qualitatively similar segmental energy scalings.[55,56] Studies of the *n*-alkanes adsorbed on $Al_2O_3(0001)$ suggest that the values of adsorbate−substrate interactions decrease with increasing chain length.[55] On the basis

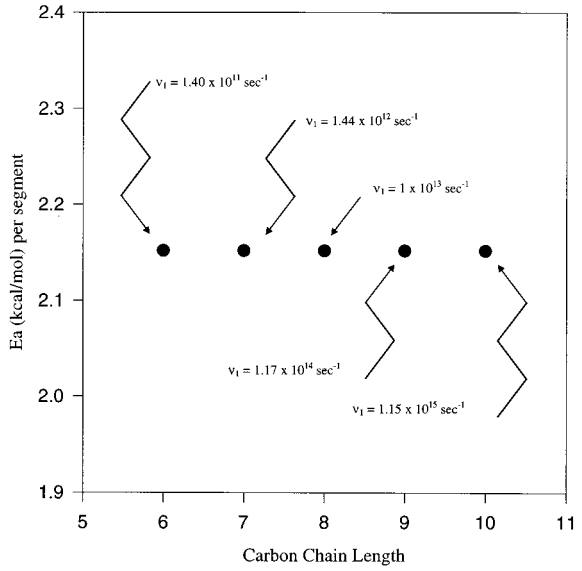

Figure 13. Variation in an assumed preexponential factor necessary to compensate for the scaling of the segmental interaction energies observed in first-order desorption fits for the TPD of *n*-alkane monolayers on Pt(111).

of a first-order fit to TPD data, desorption energies of 8.4 kcal/mol for *n*-butane, 10.4 kcal/mol for *n*-hexane, and 14.6 kcal/mol for *n*-octane were obtained (which from a simple analysis suggests a segmental interaction energy of 2.1, 1.7, and 1.8 kcal/mol, respectively). Laser-induced thermal desorption of *n*-alkanes adsorbed on Ru(001) also found a complex chain-length-dependent scaling of activation energies for desorption.[56] Propane required 11.0 kcal/mol for desorption, *n*-butane 11.9, *n*-pentane 13.8, and *n*-hexane 15.0. If these values are scaled by the chain length, one estimates the average segmental activation energies as being 3.67 kcal/mol for propane, 2.96 for *n*-butane, 2.76 for *n*-pentane, and 2.50 for *n*-hexane.

In gross terms, one might rationalize these behaviors in the context of different binding affinities for methyl and methylene groups, namely, that the methyl group is more strongly bound (on Pt, for example) than is the methylene. The present data (Figure 12) requires that this binding difference (between CH_3 and chain interior CH_2 groups) be as large as a factor of 6 to account for the chain-length-dependent energy scaling seen across the C_6-C_{10} series. A factor this large seems physically implausible to us. The nature of this desorption process thus appears to be more complex than that approximated by a simple analysis of the desorption temperatures as given by eq 2.

Several factors might contribute to the failure of a model based on a simple first-order rate law, the most likely of which is the assumption of a chain-length-invariant preexponential factor, ν_1. A simple calculation allows us to demonstrate the range of the scaling of ν_1 needed to force a constant average segmental interaction energy across the series. Assuming as a reference value that ν_1 equals 1×10^{13} s^{-1} for *n*-octane, eq 2 implies that the preexponential factor for decane must increase by nearly 2 orders of magnitude and that for hexane decrease by nearly 2 orders of magnitude to maintain a constant segmental scaling of the activation energy for desorption (Figure 13). This hypothesis can be explicitly tested by performing the TPD experiments with a variety of temperature ramp rates (β). Experiments performed this way (with β varied between 0.08 and 3 K/s) did not support this argument: values of ν_1 for hexane, octane, and decane are found via the more elaborate Redhead formalism to be 6.9×10^{12}, 1.6×10^{13}, and 6.5×10^{12} s^{-1}, respectively (Figure 14) and thus are experimentally indistinguishable.

Other issues, such as a strong coverage dependence of either the activation energy or the preexponential factor (or both), might also be considered as being important to these rate processes.[57,58] While likely, we believe that other more fundamental factors must be considered in the context of the kinetic modeling. We ask, for example, if a model based on a simple first-order rate law is an intrinsically incorrect formalism for deducing the magnitude of the segmental interaction energies. The construction of a detailed energy balance proves instructive here. Desorption from the multilayer involves only the breaking of adsorbate−adsorbate interactions. The monolayer desorption process should include contributions that relate to both adsorbate−adsorbate and adsorbate−substrate interaction energies. We know, given the importance of an island growth mechanism in the formation of the monolayer,[29] that the lateral interactions between the chains are significant and attractive. It thus may be necessary to develop rate equations that account for these attractive lateral interactions and the mass-action principles via which they are manifested in the desorption kinetics.

As many authors have noted, the effects of lateral interactions on TPD data can be quite profound.[48,57] For example, Meng et al. have studied the effects of lateral interactions between adsorbates on desorption kinetics via Monte Carlo simulations.[59] Their results show unambiguously that such interactions strongly influence the rate profiles that would be obtained by TPD. Perhaps most important, though, this work documents the strong influences exerted by the manner in which these interactions are sampled and evolve through a changing coverage of the adsorbate.

We turn now to consider a simple kinetic model that invokes an important role for attractive lateral interactions. The simplest starting point here is to consider a rate law that describes the inverse of the growth process, the two-dimensional (2-D) sublimation of an island. The desorption of adsorbate molecules bound in a 2-D island could demonstrate a number of interesting kinetic behaviors. The simplest case, one described well in the literature,[59,60] is illustrated by the scheme given below.

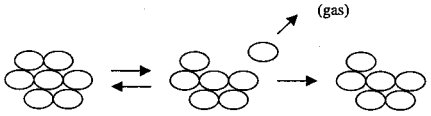

The scheme illustrates a process in which molecules can bind to domains but reversibly dissociate and occupy open lattice sites (similar to a gas−solid equilibrium). Desorption to the gas phase occurs irreversibly for some fraction of the molecules detached from the cluster. If the domain is large enough to saturate this "preequilibrium", pseudo-zero-order desorption kinetics will be obtained. The TPD line shapes obtained here do not support this limiting kinetic model.[46,48,49] A more complex version of this mechanism seems better suited to model the data, however. The important aspects of this revised model are (1) that the overlayer structure is not static and (2) that desorption might proceed from more than one distinct bound state.

We can make some approximations about the structure of the adsorbate layer and the manner in which it contributes to the desorption mechanism. Earlier studies have shown unambiguously that the molecules reside in an ordered structure as (previously shown by LEED[13] and RAIRS[29]), *one whose organizational characteristics are largely preserved up to temperatures closely approaching the desorption threshold*.[29]

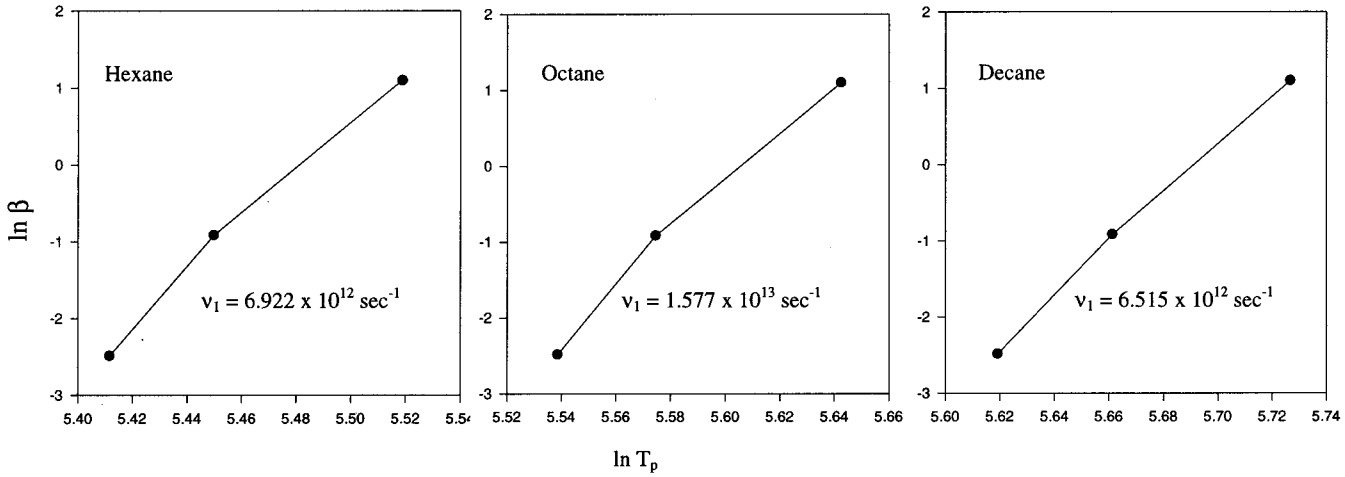

Figure 14. Variation of the peak desorption temperature as a function of temperature ramp rate as analyzed according to the Redhead method. The experimentally measured preexponential factors for *n*-hexane, *n*-octane, and *n*-decane are experimentally indistinguishable.

Further, we assume that the overlayer is comprised of domains (perhaps intrinsic or separated by terraces, edges, etc.). We then ask whether the adsorbate molecule will desorb with a greater kinetic competence from the center of a domain or its edge? Energetic arguments suggest that desorption from the dense interior of a domain will not be kinetically favorable; there are too many interactions to overcome for this to be the most facile process. One therefore looks to the domain structure to identify adsorbate binding regions with fewer lateral interactions. If the domain is characterized by some constant number of internal vacancies (e.g., as in a thermal population), it is reasonable to assume that the finite number of these defects will contribute little to the overall desorption rate.[61] If the internal defects are larger, then they will contribute to the desorption rate but in the same manner as would the perimeter of the domain. In either mechanism, we expect that the desorption process would be dominated by the loss of molecules bound along a domain perimeter, either internal or external. Raut et al. have shown in a molecular-dynamics simulation of *n*-alkanes on Pt(111) that nonfrustrated lateral diffusion is weakly activated (∼0.65 kcal/mol for *n*-butane[62] and ∼1.2 kcal/mol for *n*-octane).[63] These activation barriers are sufficiently low to reasonably conclude that diffusion will be facile relative to desorption and that large interior vacancies/voids should be rapidly filled resulting in a vacancy motion to the edge of the domain as shown in the illustration below.

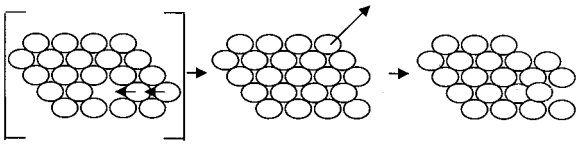

This suggests that an evaporation proceeding predominantly from the perimeter needs to be considered as the basis for constructing a model of the desorption process. We can write the instantaneous change of the coverage, θ, with respect to time in terms of such a model system. The simplest case is approximated by

$$\frac{d\theta}{dt} = -Ck_1(\sqrt{\theta}) \tag{3}$$

where the desorption rate is simply the rate of desorption from the domain edges (a more weakly bound state). The model is derived geometrically by assuming that molecules only desorb from some finite area at the perimeter of a hypothetical circular domain (where molecules experience fewer attractive lateral interactions, with the constant C collecting the geometric terms corresponding to the perimeter and domain scalings). This equation is written for a single domain; however, the resulting net desorption flux approximated in this way will simply scale as the number of domains (with attendant geometric biases not accounted for at this level of analysis). The most significant aspect to note in this model is that the desorption rate involves a half-order coverage term. We note that Nishimura et al. found a half-order desorption rate for the desorption of methanol from Al_2O_3(0001). They attribute this rate dependence to the hydrogen bonding occurring within the multilayer.[64]

Does this new model, then, provide a more sensible way to model the desorption kinetics, one that also leads to a more intuitive and physically plausible scaling (or nearly constant value) of the average segmental interaction energy? To test this qualitatively, we look at a limiting analysis based on two assumptions: (a) that the surface−segment interaction energy is constant (i.e., the methyl and methylene interaction energies are similar in magnitude and thus do not contribute to a pronounced chain-length dependence), and (b) the desorption energies, on a per segment basis, can be related via the varying contributions made by lateral interactions. The rate constant k_1 in this context is approximated by the following equation

$$k_1 = \nu_0 \exp\frac{-(\text{length})(E_{\text{seg}} + aE_{\text{sub}})}{RT} \tag{4}$$

where ν_0 is the preexponential factor, length is the number of carbon centers in the chain, E_{seg} (a constant) represents the average surface−segment interaction energy, and E_{sub} is a measure of the lateral interaction energy, as might be referenced to the desorption energy of a nonsurface-contacting state (or perhaps better, a group constituent heat of sublimation taken from the literature). The variable a refers to the multiplication factor that accounts for the fraction of lateral interactions contributing to the energy barriers for desorption of a "perimeter" molecule. For the lateral interaction energy, we use as the simplest estimate of E_{sub} a value of 2.0 kcal/mol, which is $^1/_8$ of the desorption energy calculated from the zero-order desorption fit for an octane multilayer. We are left only to substitute for E_{seg}.

We turn to the literature for guidance in choosing a value for E_{seg}. TPD studies should be sensitive to the kinetic modeling

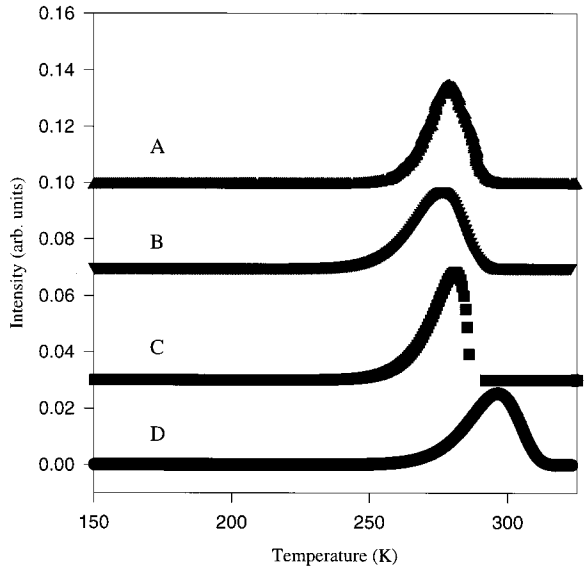

Figure 15. Fits of desorption data showing: (A) experimental TPD data for the desorption of a monolayer of octane from Pt(111); (B) first-order desorption fit corresponding with a calculated activation energy of 17.2 kcal/mol; (C) modified desorption model with a calculated activation energy of 18.5 kcal/mol (assuming a fractional contribution from lateral interactions according to the form described in eq 4); (D) desorption temperature obtained for a first-order model using a calculated activation energy of 18.5 kcal/mol.

problems noted here (see above), and the data, where available are not generally as broad as given in the present work. Using different kinetic methods, Wetterer et al. reported an extensive study of the binding energetics of a broad series of long-chain adsorbates on Au(111).[65] This study also noted an apparent chain-length-dependent scaling of the average segmental interaction energy similar to (although not as large as) that shown in Figure 12. Their data further suggest that the binding enthalpies of the *n*-alkanes on Pt(111) (as measured here) and Au(111) are very similar. If we normalize these measured binding enthalpies by the chain lengths (and, as before, neglect any asymmetry in the chain-end vs interior-segment binding energies), one obtains values of the average segmental interaction energy that range from 2.23 (*n*-C6) to 1.86 (*n*-C12) across an adsorbate series similar to that examined here. The two systems thus appear to give very similar trends (and, implicitly, a similar crossing of the (bulk) heats of sublimation and adsorption on the metal, albeit at a slightly longer chain length than was the case for our data for Pt(111)). Raut et al. calculated the binding energy for various alkanes on Pt(111) using transition-state theory and found values of 13.84 kcal/mol for *n*-hexane, 18.79 kcal/mol for *n*-octane, and 23.64 kcal/mol for *n*-decane.[63] These calculations suggest a value for the average segmental interaction energy of 2.3 kcal/mol for the adsorption of *n*-alkanes on Pt. Taken together, these studies provide a reasonable range for approximating of the contributions of the surface−segment interaction energy, and we adopt it for the calculations that follow. With the addition of contributions due to the lateral adsorbate−adsorbate interactions, values in this range serve to plausibly illustrate the scaling of the desorption energies in ways that qualitatively track the data.

Figure 15 shows a fit of the desorption model and a standard first-order model to the experimental desorption spectra for a monolayer of *n*-octane. The four traces in the figure correspond to the following: A is the experimental desorption data for octane showing desorption at approximately 277 K (monolayer); B is a first-order fit for the monolayer state following the Redhead method (giving a desorption energy of 17.2 kcal/mol); C shows the modified desorption model fitting the monolayer desorption peak at 277 K with a predicted desorption energy of 18.5 kcal/mol by assuming a constant segmental interaction energy of 2.3 kcal/mol (the upper limit suggested by theory) with a small contribution from lateral interactions of 0.01 kcal/mol (we believe this value is far too low, see below); D shows that a first-order desorption calculation using the same energy calculated by our modified model, 18.5 kcal/mol, yields a predicted desorption max at approximately 295 K. As can be seen in the figure, the revised model can be used to approximate the actual monolayer desorption kinetics reasonably well and do so without invoking a very complex (and here nonphysical) chain-length-dependent scaling of the interaction energy. We note, though, that as the chain length becomes longer the monolayer desorption features broaden substantially, and the line shapes we calculate do not match as accurately. It is important to note that this model is far too simple to form the basis of a revised quantitative model. For example, we believe it is likely that the desorption process is mediated by a desorption precursor state. The addition of a precursor state(s) to the model will complicate significantly any simulation of the line shapes.[66] While the inclusion of a precursor would allow a more accurate modeling of the desorption process, it is beyond the scope of the simple kinetics invoked in this discussion. In principle, the fits to the spectra also could be more forcefully constrained to fit the entire data set. There appears to be little advantage gained in doing so, however, as these solutions are not uniquely determinate. It follows from the model that other scaled values of the surface−segment and chain−chain interaction energies can be used here equally well if we adopt other estimated values from the literature. For example, if we assume a surface−segment interaction energy of 1.90 kcal/mol (our lower limit from above), one obtains an identical simulation for a larger contribution of $aE_{sub} = 0.51$ kcal/mol. The more important point we infer from this exercise is that a simple geometric model can account for the mass-action kinetics seen in this prototypical overlayer system. The more subtle point developed in the current discussion, though, is that there still exists a need to develop a chain-length-dependent energy scaling. Rather than have this occur in the average surface−segment interaction energy (which as we saw leads to nonphysical results), we have this arise more naturally via the relative contributions made by lateral interactions. The model described here requires that the value of the constant C increases with the chain length in order to quantitatively account for the progression seen in the peak maxima. Since this parameter contains geometric terms relating to the domain structure, this inference seems to us to be more plausible physically than the alternative possibilities described above. We note that an earlier study reported by us provides inferential support for this model. In that work we found that a mixed monolayer of cyclooctane with *n*-octane-d_{18} shows two distinct states for the desorption of the cyclooctane; one is seen at the normal peak desorption temperature for cyclooctane (250 K) and the other at a higher temperature appropriate for the *n*-alkane (275 K). This strongly argues that domain effects are weighted in the TPD data. Some limitations not mentioned above are also evident in the model. Perhaps most critical is the degree to which first- and half-order processes might be occurring competitively. This latter factor is critical for understanding the nature of the kinetics contributing at both early and late times in the TPD rate profile. This complication not withstanding, we believe that even at this crude level of development the results are suf-

ficiently encouraging to warrant further study by both computational and more precise experimental means.

Acknowledgment. We acknowledge Professor Dan Schwartz for insightful discussions. We gratefully acknowledge the support of the National Science Foundation (CHE-9626871).

References and Notes

(1) Cullis, P. R.; Hope, M. J. *Biochemistry of Lipids, Lipoproteins and Membranes;* Vance, D. E., Vance, J., Eds.; Elsevier Science Publishers: New York, 1991.
(2) Israelachvilli, J. N. *Intermolecular and Surface Forces*; Academic Press: London, 1985.
(3) Roberts, G. G. *Langmuir−Blodgett Films*; Plenum Press: New York, 1990.
(4) Barlow W. A. *Langmuir−Blodgett Films*; Elsevier Scientific Publishers: New York, 1980.
(5) Nuzzo, R. G.; Allara, D. L. *J. Am. Chem. Soc.* **1983**, *105*, 44881−4483.
(6) Dubois, L. H.; Nuzzo, R. G. *Annu. Rev. Phys. Chem.* **1992**, *43*, 437.
(7) Mathisen, H.; Norman, N.; Pedersen, B. F. *Acta Chem. Scand.* **1967**, *21*, 127−135.
(8) Segerman, E. *Acta Cryst.* **1965**, *19*, 789−796.
(9) Norman, N.; Mathisen, H. *Acta Chem. Scand.* **1972**, *26*, 3913−1916.
(10) Hstie, G. P.; Roberts, K. J. *J. Mater. Sci.* **1994**, *29*, 1915−1919.
(11) Mirkin, N. G.; Krimm, S. *J. Phys. Chem.* **1993**, *97*, 13887−13895.
(12) Hammonds, K. D.; McDonald, I. R. *Chem. Phys. Lett.* **1993**, *213*, 27−31.
(13) Firment, L. E.; Somorjai, G. A. *J. Chem. Phys.* **1977,** *66*, 2901−2913.
(14) Wu, X. Z.; Sirota, E. B.; Sinha, S. K.; Ocko, B. M.; Deutsch, M. *Phys. Rev. Lett.* **1993**, *70*, 958−961.
(15) Maroncelli, M.; Strauss, H. L.; Snyder, R. G. *J. Chem. Phys.* **1985**, *82*, 2811−2824.
(16) Nozaki, K.; Higashitani, N.; Yamamoto, T.; Hara, T. *J. Chem. Phys.* **1995**, *103*, 5762−5766.
(17) Sirota, E. B.; Singer, D. M. *J. Chem. Phys.* **1994**, *101*, 10873−10882.
(18) Sirota, E. B.; King, H. E., Jr.; Shao, H. H.; Singer, D. M. *J. Phys. Chem.* **1995**, *99*, 798−804.
(19) McClure, D. W. *J. Chem. Phys.* **1968**, *49*, 1830−1839.
(20) Hoffman, J. D. *J. Chem. Phys.* **1952**, *20*, 541−549.
(21) Ungar, G. *J. Phys. Chem.* **1983**, *87*, 689−695.
(22) Casal, H. L.; Mantsch, H. H.; Cameron, D. G.; Snyder, R. G. *J. Chem. Phys.* **1982**, *77*, 2825−2830.
(23) Sirota, E. B.; Singer, D. M.; King, H. E., Jr. *J. Chem. Phys.* **1994**, *100*, 1542−1551.
(24) Barnes, J. D.; Fanconi, B. M. *J. Chem. Phys.* **1972**, *56*, 5190−5192.
(25) Sirota, E. B.; King, H. E., Jr.; Singer, D. M.; Shao, H. H. *J. Chem. Phys.* **1993**, *98*, 5809−5824.
(26) Ungar, G.; Masic, N. *J. Phys. Chem.* **1985**, *89*, 1036−1042.
(27) Maroncelli, M.; Qi, S. P.; Strauss, H. L.; Snyder, R. G. *J. Am. Chem. Soc.* **1982**, *104*, 6237−6247.
(28) Kim, Y.; Strauss, H. L.; Snyder, R. G. *J. Phys. Chem.* **1989**, *93*, 7520−7526.
(29) Hostetler, M. J.; Manner, W. L.; Nuzzo, R. G.; Girolami, G. S. *J. Chem. Phys.* **1995**, *99*, 15269−15278.
(30) Zerbi, G.; Magni, R.; Gussoni, M.; Moritz, K. H.; Bigotto, A.; Dirlikov, S. *J. Chem. Phys.* **1981**, *75*, 3175−3194.
(31) Clavell-Grunbaum, D.; Strauss, H. L.; Snyder, R. G. *J. Chem. Phys. B* **1997**, *101*, 335−343.
(32) Bishop, A. R.; Hostetler, M. J.; Girolami, G. S.; Nuzzo, R. G. *J. Am. Chem. Soc.* **1998**, *120*, 3305−3315.
(33) Wiegand, B. C.; Lohokare, S. P.; Nuzzo, R. G. *J. Phys. Chem.* **1993**, *97*, 11553−11562.
(34) Nuzzo, Dubois, L. H.; Allara, D. L. *J. Am. Chem. Soc.* **1990**, *112*, 558−569.
(35) Gadzuk, J. W. *Excitation Mechanisms in Vibrational Spectroscopy of Molecules on Surfaces*; Plenum Press: New York, 1987; Vol. 1, pp 49−104.
(36) Woodruff, D. P.; Delchar, T. A. *Modern Techniques of Surface Science*; Cambridge University Press: New York, 1992; pp 414−437.
(37) Manner, W. L.; Bishop, A. R.; Girolami, G. S.; Nuzzo, R. G. *J. Phys. Chem. B* **1998**, *102*, 8816−8824.
(38) MacPhail, R. A.; Strauss, H. L.; Snyder, R. G.; Elliger, C. A. *J. Phys. Chem.* **1984**, *88*, 334−341.
(39) Snyder, R. G.; Scherer, J. R. *J. Chem. Phys.* **1979**, *71*, 3221−3228.
(40) Tasumi, M.; Shimanouchi, T. *J. Chem. Phys.* **1965**, *43*, 1245−1258.
(41) Snyder, R. G. *J. Mol. Spectrosc.* **1961**, *7*, 116−144.
(42) Hutchinson, J. S.; Hynes, J. T.; Reinhardt, W. P. *J. Phys. Chem.* **1986**, *90*, 3528−3532.
(43) Snyder. R. G. *J. Chem. Phys.* **1979**, *71*, 3229−3235.
(44) Smith, A. E. *J. Chem. Phys.* **1953**, *21*, 2229.
(45) At this temperature, self-diffusion is expected to be very slow.
(46) Somorjai, G. A. *Introduction to Surface Chemistry and Catalysis*; John Wiley and Sons: New York, 1994; pp 60−61.
(47) Argile, C.; Rhead, G. E. *Surf. Sci. Rep.* **1989**, *10*, 277.
(48) King, D. A. *Surf. Sci.* **1975**, *47*, 384−402.
(49) Chan C.-M.; Aris, R.; Weinberg, W. H. *Appl. Surf. Sci.* **1978**, *1*, 360−376.
(50) Russell, N. M.; Ekerdt, J. G. *Surf. Sci.* **1996**, *364*, 199−218.
(51) The intensity of the mass spectrometer signal is related to both the desorbing flux and an instrument response factor; this later nonexponential term is incorporated into the apparent magnitude of the preexponential factor.
(52) Lide, D. R. *Handbook of Chemistry and Physics*; CRC Press: Boca Raton, FL, 1991.
(53) Sexton, B. A.; Hughes, A. E. *Surf. Sci.* **1984**, *140*, 227−248.
(54) Redhead, P. A. *Vacuum* **1962**, *12*, 203.
(55) Slayton, R. M.; Aubuchon, C. M.; Camis, T. L.; Noble, A. R.; Tro, N. J. *J. Phys. Chem.* **1995**, *99*, 2151−2154.
(56) Brand, J. L.; Arena, M. V.; Deckert, A. A.; George, S. M. *J. Chem. Phys.* **1990**, *92*, 5136−5143.
(57) de Jong, A. M.; Neimantsverdriet, J. W. *Surf. Sci.* **1990**, *233*, 355−365.
(58) Wittrig, T. S.; Ibbotson, D. E.; Weinberg, W. H. *Appl. Surf. Sci.* **1980**, *4*, 234−237.
(59) Meng, B.; Weinberg, W. H. *J. Chem. Phys.* **1994**, *7*, 5280−5289.
(60) Meng, B.; Weinberg, W. H. *Surf. Sci.* **1997**, *374*, 443−453.
(61) To maintain a thermal population of vacancies in such a process, lateral diffusion, which is know to be facile, would collapse the divacancy and thus contract to the domain.
(62) Raut, J. S.; Sholl, D. S.; Fichthorn, K. A. *Surf. Sci.* **1997**, *389*, 88−102.
(63) Raut, J. S.; Fichthorn, K, A. *J. Chem. Phys.* **1998**, *4*, 1626−1635.
(64) Nishimura, S. Y.; Gibbons, R. F.; Tro, N. J. *J. Phys. Chem. B* **1998**, *102*, 6831−6834.
(65) Wetterer, S. M.; Lavrich, D. J.; Cummings, T.; Bernasek, S. L.; Scoles, G. *J. Phys. Chem. B* **1998**, *102*, 9266−9275.
(66) Bamford, C. H.; Tipper, C. F. H.; Compton, R. G. *Comprehensive Chemical Kinetics Simple Processes at the Gas−Solid Interface*; Elsevier Press: Amsterdam, 1984.